ARTICLE

# Ultrafast Dynamics Through Conical Intersections in 2,6-dimethylpyridine Studied with Time-resolved Photoelectron Imaging†

Xue-jun Qiu[a], Rong-shu Zhu[b], Yan-qi Xu[a], Abulimiti Bumaliya[a], Song Zhang[a], Bing Zhang[a]*

*a. State Key Laboratory of Magnetic Resonance and Atomic and Molecular Physics, Wuhan Institute of Physics and Mathematics, Chinese Academy of Sciences, Wuhan 430071, China; Graduate School of the Chinese Academy of Sciences, Beijing 100049, China*

*b. Environmental Science and Engineering Research Center, Harbin Institute of Technology Shenzhen Graduate School, Shenzhen 518055, China*

(Dated: Received on August 2, 2011; Accepted on August 29, 2011)

The ultrafast dynamics through conical intersections in 2,6-dimethylpyridine has been studied by femtosecond time-resolved photoelectron imaging coupled with time-resolved mass spectroscopy. Upon absorption of 266 nm pump laser, 2,6-dimethylpyridine is excited to the $S_2$ state with a $\pi\pi^*$ character from $S_0$ state. The time evolution of the parent ion signals consists of two exponential decays. One is a fast component on a timescale of 635 fs and the other is a slow component with a timescale of 4.37 ps. Time-dependent photoelectron angular distributions and energy-resolved photoelectron spectroscopy are extracted from time-resolved photoelectron imaging and provide the evolutive information of $S_2$ state. In brief, the ultrafast component is a population transfer from $S_2$ to $S_1$ through the $S_2/S_1$ conical intersections, the slow component is attributed to simultaneous IC from the $S_2$ state and the higher vibrational levels of $S_1$ state to $S_0$ state, which involves the coupling of $S_2/S_0$ and $S_1/S_0$ conical intersections. Additionally, the observed ultrafast $S_2 \rightarrow S_1$ transition occurs only with an 18% branching ratio.

**Key words:** 2,6-dimethylpyridine, Photoelectron imaging, Conical intersection, Internal conversion, Time-resolved spectroscopy

## I. INTRODUCTION

The Born-Oppenheimer approximation, an adiabatic separation of electronic and vibrational motions, is exact if the nuclear kinetic energy is negligible. However, the adiabatic or Born-Oppenheimer single potential energy surface approximation is valid for the most of dynamics processes due to the motions of the atoms and occurs at the intersections or near intersections of potential energy surfaces belonging to different electronic states [1]. These dynamics processes are dominated by the nonadiabatic transitions, which lead to coupling of potential energy surfaces and extend nuclear motion to more than one Born-Oppenheimer potential energy surface, are playing a significant role in many polyatomic molecule. This multidimensional potential energy surfaces can undergo conical intersection, which have one geometry of the crossing region between electronic states resembling the vertex of a right circular cone and the two conical surfaces smoothly connecting through a point [2]. The conical intersection, inducing ultrafast internal conversion (IC), has been implicated in many photochemistry and photobiological processes [3] and underlies many concepts in molecular electronics [4]. Although conventional approaches such as fluorescence lifetime and quantum yield measurements provide fundamental information on nonadiabatic processes [5], direct observation of the nonstationary state is by far more informative for disentangling their complex dynamics.

Recently-developed time-resolved photoelectron imaging (TRPEI) has been proven to be a powerful technique in this regard [6, 7]. The TRPEI translates into the photoionization differential cross section, energy resolved to within the probe bandwidth. It thus provides both the energy and the angular distribution of the photoelectrons as well as their correlation as a function of time. In particular, the sensitivity of the photoelectron angular distribution to the electronic symmetry translates into useful information regarding the discrimination and visualization of wave packet dynamics.

Pyridine and its methyl derivatives are important heteroaromatic molecules, which have attracted a great deal of attention over the last two decades [8−11] due to their important roles in the UV photodamage of

†Part of the special issue for "the Chinese Chemical Society's 12th National Chemical Dynamics Symposium".

*Author to whom correspondence should be addressed. E-mail: bzhang@wipm.ac.cn, FAX: +86-27-87198491

 

nucleic acids [12]. A recent study of pyridine carried out by Zewail and Chachisvilis shows that the $S_2$ ($\pi\pi^*$) state of pyridine undergoes a photoisomerization to prefulvenic form identified as a main product in this reaction [8]. They conclude that this molecule structurally relaxes in hundreds of femtosecond or less, and then crosses the barrier of $S_2$ state to reach the ground state of prefulvene through the conical intersection. It is expected that methyl substitution in the 2- and 6-positions of pyridine will have significant effects on the topology of the relevant conical intersections, on the basis of previous theory and experience with the methyl substituted. Peyerimhoff and coworkers have predicted this molecule is the most stable isomer [13], using density functional theory, CASSCF, CASPT2, and MRCI. The presence of two methyl groups in the 2- and 6-positions of pyridine further stabilizes the ring through increased charge density [14]. Zewail and coworkers have eliminated the possibility of a ring opening isomerization process in 2,6-dimethylpyridine [15]. Therefore, from the $S_2$ state of 2,6-dimethylpyridine, only four deactivation processes are proposed: $S_2$-$S_0$ fluorescence decay, $S_2$-T intersystem crossing, $S_2$-$S_1$ IC and $S_2$-$S_0$ IC. The very small fluorescence quantum yield implies that the first process can be neglected [16, 17]. Furthermore, Sushida *et al.* reported that at 266 nm, 2,6-dimethylpyridine excited to the $S_2$ state and underwent IC back to $S_0$ with a lifetime of 7 ps [16]. In addition, Park *et al.* have shown that the IC to $S_0$ occurs in about 4 ps [18]. However, addition of electron-donating methyl substituents tends to shrink the gap between the first ($n\pi^*$) and second ($\pi\pi^*$) excited states [15], which leads to an enhanced $S_2$-$S_1$ IC in 2,6-dimethylpyridine [9, 19]. These notable discrepancies warrant the further studied the ultrafast dynamics of $S_2$ state in 2,6-dimethylpyridine to gain deeper insight using femtosecond time-resolved photoelectron imaging.

In this work, we presented a short communication on nuclear wave-packet dynamics on multidimensional potential energy surfaces of 2,6-dimethylpyridine by TR-PEI. We focus primarily on time-resolved photoelectron kinetic energy (PKE) distributions and photoelectron angular distributions (PADs) to investigate ionization dynamics from the $S_2$ and $S_1$ as well as the dynamics processes of $S_2$ state through conical intersections.

## II. EXPERIMENTS

The details of our femtosecond (fs) laser system have been described elsewhere [20]. Briefly, the seed beam was generated by a commercial Ti:sapphire oscillator pumped by a CW second harmonic of an Nd:$YVO_4$ laser, and then amplified by an Nd:YLF pumped regenerative amplifier to generate a 1 kHz pulse train centered at 800 nm (with a 30 nm bandwidth, 45 fs pulse width) with maximum energy of 1 mJ/pulse. This light was split into two equal intensity beams, one of which was frequency tripled to 267 nm, generated in a 0.2 mm thick BBO crystal by sum frequency mixing of the second harmonic and the fundamental, to produce the pump light. The other beam was served as the probe light. The probe beam was temporally delayed relative to the pump beam by a computer-controlled linear translation stage (PI, M-L01.4A1). The two laser beams were introduced into the vacuum chamber collinearly with a dichroic mirror, and focused with fused silica lens of $f$=500 and 350 mm, respectively. The polarizations of both beams were parallel to the detector plane. During experiments, typical pulse energies were about 0.3 μJ/pulse for the pump and about 48 μJ/pulse for the probe pulse.

The velocity map imaging setup [21] is similar to that designed by Eppink and Parker [22]. It consists of a molecular-beam source chamber and an ionization-flight detection chamber. The detection chamber was kept below 50 μPa with the molecular beam on. 2,6-dimethylpyridine (99.9% purity) seeded in He was expanded into the source chamber with a stagnation pressure of 202 kPa through a pulsed nozzle (general valve, with a 0.5 mm orifice) with the repetition rate of 10 Hz. The supersonic molecular beam is collimated by a conical skimmer and intersects perpendicularly with the two laser beams in a two-stage ion lens region. Photoelectrons are extracted into a 36 cm field-free region, which is doubly shielded against stray magnetic fields by μ-metal tube. At the end of the time-of-flight tube, the electrons strike a two-stage microchannel plate detector backed by a phosphor screen. The images on the screen are captured with a thermoelectrically cooled charge-coupled-device video camera (LAVISION Inc., Imager Intense). Each photoelectron image is integrated more than $10^4$ laser shots. The emission from the phosphor screen is monitored by a photomultiplier connected to a 1 GS/s digital phosphor oscilloscope (Tektronix Inc., TDS2012B) USB interfaced with a computer. A basis-set expansion (BASEX) transform [23] is applied to calculate the slices through the three-dimensional (3D) scattering distributions of the photoelectrons from the observed 2D projection images.

## III. RESULTS AND DISCUSSION

The mass spectrum of 2,6-dimethylpyridine is obtained when the pump and probe beams are temporally and spatially overlapped. It has three major peaks corresponding to $C_5H_3N^+$, $C_6H_6N^+$, and $C_7H_9N^+$, respectively. The integral area ratio of $C_7H_9N^+$, $C_6H_6N^+$, and $C_5H_3N^+$ is 44:2:1. Moreover, it is believed that most of the $C_6H_6N^+$ and $C_5H_3N^+$ originate from the dissociation of $C_7H_9N^+$ parent ion since the time-dependent ion signals of $C_6H_6N^+$ and $C_5H_3N^+$ have very similar trend to that of parent ion. Therefore, the contribution to the total photoelectron signals from the generation of $C_6H_6N^+$ and $C_5H_3N^+$ can be neglected.

DOI:10.1088/1674-0068/24/05/551-556 

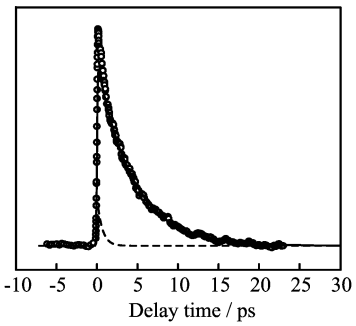


FIG. 1 Time-resolved total ion signals of parent ion as a function of delay time between the pump pulse at 267 nm and the probe pulse at 800 nm. The circles represent the experimental results, and the dash line and solid line represent the fitting results.

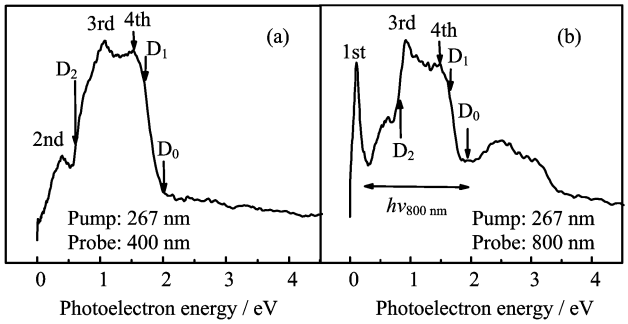


FIG. 2 PKE distributions extracted from the image at $\Delta t$=0 for different probe wavelengths. (a) Two-photon absorption of 400 nm probe pulse. (b) Four-photon absorption of 800 nm probe pulse

Figure 1 shows the observed pump-probe time profile of the photoionization signal intensity. The decay profile is fitted with the sum of two exponentials with lifetimes of $\tau_1$=635 fs and $\tau_2$=4.37 ps convoluted with a Gaussian describing the instrument response function (Gaussian with 150 fs FWHM). The former reflects the ultrafast decay from $S_2$ to $S_1$ state, whereas the latter reflects a slow IC to the ground state from $S_1$ and $S_2$. The dynamics of these decays will be discussed in details later by analysis of the photoelectron images.

In Fig.2, we present photoelectron spectra at $\Delta t$=0 extracted from images following excitation of 2,6-dimethylpyridine with femtosecond laser light at 267 nm. The probe wavelength is centered at 400 and 800 nm respectively. The adiabatic ionization energy (IE) of 2,6-dimethylpyridine is determined to be 71543 $cm^{-1}$ (8.87 eV) via photoionization mass spectrometry [24]. The initially excited $S_2$ state can be ionized by absorbing at least three probe photons at 800 nm or two probe photons at 400 nm, reaching a total energy of about 9.28 or 10.84 eV which is about 0.41 or 1.97 eV above the 2,6-dimethylpyridine adiabatic IE. The PKE bands around 1.97, 1.56, and 0.81 eV are expected for ionization to the zero vibrational level of the ionic ground state ($D_0$), the first excited state ($D_1$), and the second excited state ($D_2$) [25], by two-photon absorption of 400 nm probe pulse in Fig.2(a) or by four-photon absorption of 800 nm probe pulse in Fig.2(b). These bands centered at 0.11, 0.64, 1.00, and 1.42 eV are assigned as the first, second, third, and fourth band, which indicate that only the first band can be ionized by three-photon at 800 nm due to its disappearance in Fig.2(a). The PKE located at 0.41 eV is assigned to the $D_0 \leftarrow S_2$ ionization processes without any excess vibrational energy, by three-photon at 800 nm. According to the Franck-Condon principle, the second band in the PKE distributions can be assigned to the $D_2 \leftarrow S_2$ ionization processes, by four-photon absorption at 800 nm. The third band and fourth band can be distinguished from the following time-dependence PKE distributions, and are assigned to the $D_1 \leftarrow S_1$ and $D_1 \leftarrow S_2$. We notice that these small differences (about 0.16 eV) in the PKE of the second band, third band, and $D_2$ between Fig.2 (a) and (b) can be related to the bandwidth of different probe laser (6 nm FWHM for 400 nm, 30 nm FWHM for 800 nm), also the error between the measured PKE and expected energy is considered acceptable under this condition.

Figure 3 shows representative snapshots of the photoelectron images which are the slices through three-dimensional photoelectron distributions in the plane with the polarization axis of the lasers. The time-dependence PKE distributions are extracted from a series of images. A difference PKE distribution between nonzero and zero delay time are shown in Fig.4, where $\Delta I$ is expressed as $\Delta I = I_{\Delta t \neq 0} - I_{\Delta t=0}$, $\Delta t$ and $I$ are the pump-probe delay time and the normalized intensity of PKE distribution. $\Delta I$=0 is regarded as a benchmark to reflect the increase ($\Delta I$>0) and decrease ($\Delta I$<0) of the intensity at $\Delta t \neq 0$ relative to $\Delta t$=0 in the time-dependence PKE distributions. In Fig.4(a), It can be characterized by a rapid decay of electrons corresponding to first, second, and fourth band, while soft growth in the electrons corresponding to the third band during the first 630 fs. This rapid decay and energy transfer represent the fast component with a time constant of 635 fs, all photoelectron bands decrease slowly together at the similar rate after 630 fs, which is shown in Fig.4(b), and this slow decay represents to the second component with a time constant of 4.37 ps.

The band origin of the $S_0$-$S_2$ transition in 2,6-dimethylpyridine is at 271 nm [18, 26], so upon absorption of 266 nm pump laser, 2,6-dimethylpyridine is excited to the $S_2$ state. There is no significant long-lived component observed in the presented work suggesting that the $S_2$-T crossing quantum yield should be very low. According to the discussion above, the first, second, and fourth band is due to ionization of the populated $S_2$ state, which may relax down to the vibrationally excited $S_1$ and $S_0$ states by rapid IC. The changes in the integral intensity of each photoelectron

DOI:10.1088/1674-0068/24/05/551-556 

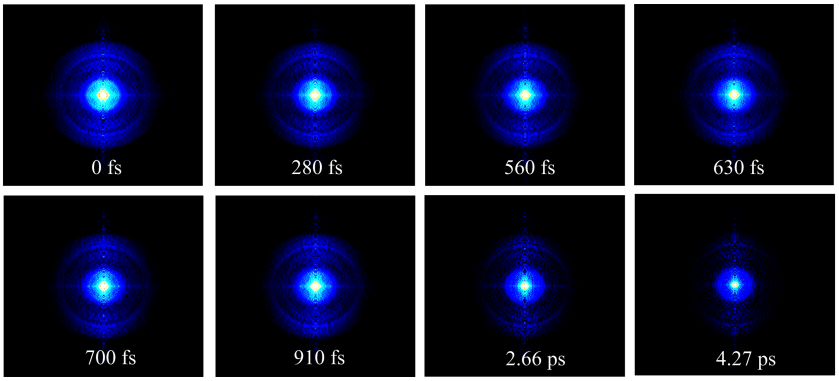


FIG. 3 A series of time-resolved BASEX-inverted photoelectron images of 2,6-dimethylpyridine observed using a pump laser wavelength of 267 nm and a probe wavelength of 800 nm. The linear polarizations of the pump and probe lasers are aligned vertical in the plane of the figure.

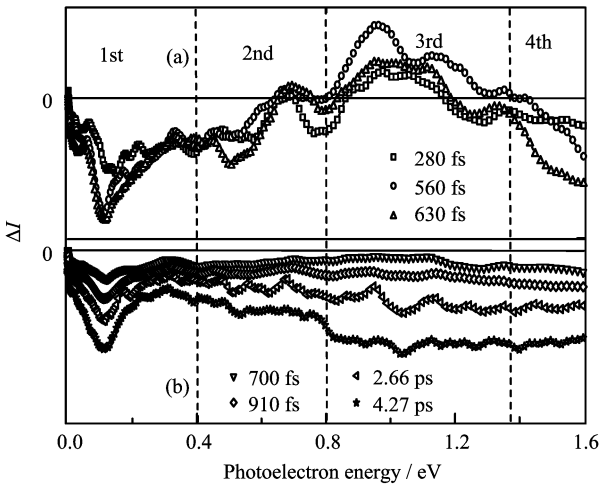


FIG. 4 A difference PKE distribution between nonzero and zero delay time. The solid line $\Delta I$=0 is regarded as a benchmark to reflect the increase ($\Delta I$>0) and decrease ($\Delta I$<0) of the intensity at $\Delta t \neq 0$ relative to $\Delta t$=0 in the time-dependence PKE distributions.

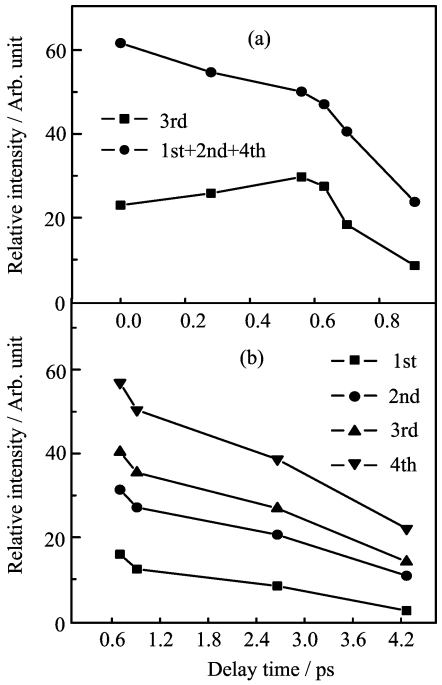


FIG. 5 Time-dependent photoelectron band integral yields for 1st, 2nd, 3rd, and 4th at special delay time from 0 fs to 4.27 ps.

band with different delay time are shown in Fig.5. It can be seen more clearly from Fig.5(a) that integral intensity for the sum of the first, second and fourth band decays rapidly during the first 630 fs, which indicates populated $S_2$ state undergoes an IC into vibrationally excited level of $S_1$ state. Its order of magnitude is 630 fs, which is in excellent agreement with the time-dependence of the ion signal. The third band grows slightly as delay time increases from 0 fs to 630 fs, as shown in Fig.5(a). Its appearance is due to population of the $S_1$ state by IC from the $S_2$ state.

All photoelectron bands decrease slowly at the similar rate after 630 fs in Fig.5(b). A deactivation mechanism for the $S_2$ state has been proposed from experiments that $S_2$ state populated transfer from $S_2$ to $S_1$ during the first 630 fs. Subsequent dynamics invokes the $S_2/S_0$ and $S_1/S_0$ conical intersections, which lead to the IC to the ground state from the $S_2$ and $S_1$ state. However, the corresponding Franck-Condon factors between the ground state with high vibrational levels and the cation states are extremely poor. The secondary population of the ground state has not been observed in our pump-probe experiments. Yamazaki *et al.* have investigated the vapor-phase fluorescence emissions yield of 2,6-dimethylpyridine is fairly constant throughout the $S_1 \leftarrow S_0$ and $S_2 \leftarrow S_0$ absorption regions, and they concluded that the constancy of this value can be related to a much smaller energy gap between the $S_1$ and $S_2$ states [17]. Therefore, it's possible that the slow decay component is the superposition of IC from $S_1$ and $S_2$ to

DOI:10.1088/1674-0068/24/05/551-556 

$S_0$, which perhaps leads to the difference between the slow lifetime measured in our experiment and reported by Sushida [16] and Park [18].

The decay process of the populated $S_2$ state is attributed to simultaneous IC from the $S_2$ state to higher vibrational levels of $S_1$ and $S_0$ state with the latter being the dominant mechanism. The $S_2 \rightarrow S_1$ transition occurs only with a small branching ratio of 18% which can be estimated from the relative strengths of the ion signals [27, 28] in Fig.1. Equal ionization efficiencies were assumed for the $S_2$ and the $S_1$ state in 2,6-dimethylpyridine, an assumption which appears justified in view of the broad Franck-Condon regions in PKE distributions from 0.81 eV to 1.56 eV showing an weak dependence of the transition probabilities on the different excited state [28]. All the ionization mechanism and IC dynamics analyzed here are shown in Fig.6.

In our experimental configuration with the linear and parallel polarization of the pump and probe laser beams, the laboratory frame PADs resulting from ionization can be expanded as [29],

$$I(\theta;t) = \sigma(t)[1 + \beta_2(t)P_2(\cos\theta) + \beta_4(t)P_4(\cos\theta) + \beta_6(t)P_6(\cos\theta) + \beta_8(t)P_8(\cos\theta) + \beta_{10}(t)P_{10}(\cos\theta)] \quad (1)$$

where $\sigma(t)$ is the integral cross section, $\beta_l(t)$ is the anisotropy parameter, $P_l(\cos\theta)$ is Legendre polynomial, and $\theta$ is the angle between the laser polarization direction and the electron recoil direction. We found from $\beta_4$ to $\beta_{10}$ to be negligible. The symmetry species of the outgoing electron change, the symmetry species of the initial excited state maybe also change in order that the product remain (or contain) the totally symmetric species. It is the PADs that relate to the symmetry species of the outgoing electron, therefore, the PADs are sensitive to changes in the symmetry of the excited-state electronic wave function associated with the non-adiabatic dynamics and could provide complementary information to energy-resolved photoelectron spectroscopy. In our results, no significant changes of PADs of the first and second band are observed at different delay time.

We concluded that these two bands are from the ionization of excited state with pure symmetric species, and therefore it's confirmed that the ionization from $D_0 \leftarrow S_1$ and $D_2 \leftarrow S_1$ is impossible. However, the third and fourth band overlap too much, and it is difficult to get their PADs accurately. PADs with distributions of PKE from 0.81 eV to 1.56 eV which contain the third band and fourth band change gradually from delay time of 0 fs ($\beta_2$=0.53) to 630 fs ($\beta_2$=0.64). Hence, the time evolution of PADs with distributions of PKE of 0.81 eV to 1.56 eV reveals the third band and fourth band in PKE distributions involve different symmetry species of excited state in 2,6-dimethylpyridine, which predict the ultrafast IC from $S_2$ ($B_2$) state to $S_1$ ($B_1$) state. These interpretations are in good agreement with the discussion from time-resolved PKE distributions above mentioned.

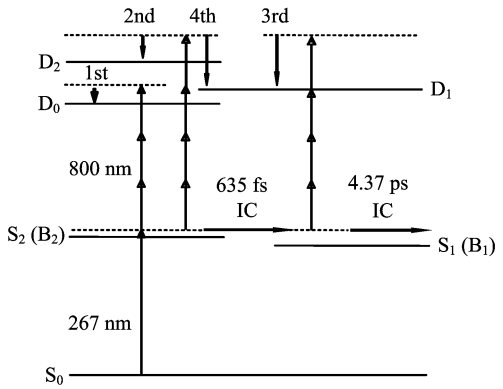


FIG. 6 Energy excitation scheme of the ground, excited, and ionic states of 2,6-dimethylpyridine. The pump laser (267 nm) prepares the $S_2$ state. Due to ultrafast IC, this state converts to the lower-lying state $S_1$ and $S_0$ with higher vibrational energy. Here, 1st, 2nd, 3rd, and 4th are corresponding to the first, second, third, and fourth band marked on Fig.2.

## IV. CONCLUSION

We have studied the ultrafast dynamics through conical intersections in 2,6-dimethylpyridine using femtosecond time-resolved photoelectron imaging coupled with time-resolved mass spectroscopy. Our results suggest that 2,6-dimethylpyridine undergoes photophysical process involving IC instead of the formation of the prefulvenic in pyridine. Upon initial excitation to the $S_2$ state with a $\pi\pi^*$ character, 18% of which decays to the $S_1$ state within 635 fs. Subsequent dynamics involves the coupling of $S_2/S_0$ and $S_1/S_0$ conical intersections, which leads to the IC to the ground state from the $S_2$ and $S_1$ states, the time constant of which has been determined on a timescale of 4.37 ps. We anticipate that correlated developments in *ab initio* molecular dynamics methods will play a key role in elucidating these dynamics.

## V. ACKNOWLEDGMENTS

This work was supported by the National Natural Science Foundation of China (No.10704083), the Innovation Foundation of Chinese Academy of Sciences (No.KJCX1-YW-N30), and the Public Science and Technology Program of Shenzhen (No.SY200806260026A).

[1] G. Herzberg and H. C. Longuet-Higgins, Faraday Discuss. **35**, 77 (1963).

DOI:10.1088/1674-0068/24/05/551-556 

[2] D. R. Yarkony, Rev. Mod. Phys. **68**, 985 (1996).
[3] R. W. Schoenlein, L. A. Peteanu, R. A. Mathies, and C. V. Shank, Science **254**, 412 (1991).
[4] J. Jortner and M. A. Ratner, Mole. Elect. **109**, 365 (1997).
[5] E. K. C. Lee, Adv. Photochem. **121**, 1 (1980).
[6] A. Stolow, A. E. Bragg, and D. M. Neumark, Chem. Rev. **104**, 1719 (2004).
[7] T. Suzuki, Annu. Rev. Phys. Chem. **57**, 555 (2006).
[8] M. Chachisvilis and A. H. Zewail, J. Phys. Chem. A **103**, 7408 (1999).
[9] D. P. Zhong, E. W. G. Diau, T. Bernhardt, S. De Feyter, J. D. Roberts, and A. H. Zewail, Chem. Phys. Lett. **298**, 129 (1998).
[10] K. E. Wilzbach and D. J. Rausch, J. Am. Chem. Soc. **92**, 2178 (1970).
[11] W. Roebke, J. Phys. Chem. **74**, 4198 (1970).
[12] C. E. Crespo-Hernandez, B. Cohen, P. M. Hare, and B. Kohler, Chem. Rev. **104**, 1977 (2004).
[13] Z. X. Cao, Q. Zhang, and S. D. Peyerimhoff, Chem. Eur. J. **7**, 1927 (2001).
[14] S. Porcinai and P. Foggi, Nuovo Cimento Soc. Ital. Fis. D **19**, 889 (1997).
[15] R. Srinivasan, J. S. Feenstra, S. T. Park, S. J. Xu, and A. H. Zewail, Science **307**, 558 (2005).
[16] K. Sushida, I. Yamazaki, and H. Baba, Oyo Denki Kenkyusho Hokoku **32**, 36 (1980).
[17] I. Yamazaki, K. Sushida, and H. Saba, J. Chern. Phys. **71**, 381 (1979).
[18] J. Park, K. Werner, and A. S. Mullin, J. Chem. Phys. **117**, 5221 (2002).
[19] E. C. Lim, Adv. Photochem. **23**, 165 (1997), and references therein.
[20] Y. Z. Liu, B. F. Tang, S. Zhang, and B. Zhang, Opt. Express **18**, 5791 (2010).
[21] Z. R. Wei, F. Zhang, Y. M. Wang, and B. Zhang, Chin. J. Chem. Phys. **20**, 419 (2007).
[22] A. T. J. B. Eppink and D. H. Parker, Rev. Sci. Instrum. **68**, 3477 (1997).
[23] V. Dribinski, A. Ossadtchi, V. A. Mandelshtam, and H. Reisler, Rev. Sci. Instrum. **73**, 2634 (2002).
[24] K. Watanabe, T. Nakayama, and J. Mottl, J. Quant. Spec-trosc. Radiat. Transfer **2**, 369 (1962).
[25] C. Utsunomiya, T. Kobayashi, and S. Nagakura, Bull. Chem. Soc. Jpn. **51**, 3482 (1978).
[26] I. Yamazaki, T. Murao, T. Yamanaka, and K. Yoshihara, Faraday Discuss. **75**, 395 (1983).
[27] W. Radloff, V. Stert, Th. Freudenberg, I. V. Hertel, C. Jouvet, C. Dedonder-Lardeux, and D. Solgadi, Chem. Phys. Lett. **281**, 20 (1997).
[28] P. Farmanara, V. Stert, W. Radloff, and I. V. Hertel, J. Phys. Chem. A **105**, 5613 (2001).
[29] C. N. Yang, Phys. Rev. **74**, 764 (1948).

DOI:10.1088/1674-0068/24/05/551-556 